MICROSCOPY

Microscopy, 2014, 337–344
doi: 10.1093/jmicro/dfu027
Advance Access Publication Date: 14 August 2014

Review

Practical aspects of monochromators developed for transmission electron microscopy

Koji Kimoto*

Electron Microscopy Group, National Institute for Materials Science, 1-1 Namiki, Tsukuba, Ibaraki 305-0044, Japan

*To whom correspondence should be addressed. E-mail: kimoto.koji@nims.go.jp

Received 1 July 2014; Accepted 14 July 2014

Abstract

A few practical aspects of monochromators recently developed for transmission electron microscopy are briefly reviewed. The basic structures and properties of four monochromators, a single Wien filter monochromator, a double Wien filter monochromator, an omega-shaped electrostatic monochromator and an alpha-shaped magnetic monochromator, are outlined. The advantages and side effects of these monochromators in spectroscopy and imaging are pointed out. A few properties of the monochromators in imaging, such as spatial or angular chromaticity, are also discussed.

Key words: monochromator, TEM, STEM, EELS, energy resolution, spatial resolution

Introduction

Several types of monochromators have been developed for electron microscopy in this decade and are now available as a tool for material characterization. They can reduce the energy spread of incident electrons to milli-electron-volt level. Monochromators can improve a diverse range of electron microscopy techniques, including not only electron energy-loss spectroscopy (EELS) [1] but also other imaging techniques, such as transmission electron microscopy (TEM) and scanning transmission electron microscopy (STEM).

A monochromator is an electron-optical system including energy-dispersive deflectors and an energy-selecting slit, and there are many types of deflectors and their combinations, which decide the inherent performance of the instrument. The implementation of a monochromator on a microscope column is also crucial. For instance, most monochromators function at a high tension, but a few function at the earth ground, yielding different performance properties. Monochromators change the illumination conditions, such as the convergence angle; therefore, the TEM imaging properties are affected in terms of both chromatic and spatial partial coherence. Although monochromators disperse the electron source image on the energy-selecting slit, a probe-forming lens focusses the source image on the specimen in STEM imaging. Thus, the monochromator properties are also related to the STEM imaging performance from the viewpoint of not only chromatic aberration but also spatial incoherence. In short, the energy-dispersed source image on the specimen might degrade the STEM spatial resolution under an inappropriate alignment condition.

In this review, the practical aspects of monochromators as a tool for electron microscopy are briefly outlined. First, the fundamental concepts of four monochromators are outlined. Then, a few critical properties of these monochromators are pointed out through a discussion of their differences. The advantages and side effects of using these monochromators in EELS, TEM and STEM imaging are also discussed.

Basic features of four monochromators

Several monochromators developed for electron microscopy have already been studied by pioneering researchers [2–4], and manufacturers have recently provided several types of monochromators. This short review focusses on currently available monochromators used for TEM and STEM.

Table 1 outlines the four monochromators described in this review: (a) a single Wien filter monochromator developed by FEI [5–7], (b) a double Wien filter monochromator by JEOL [8], (c) an omega-shaped electrostatic monochromator by CEOS [9,10] and (d) an alpha-type magnetic monochromator by NION [11,12]. Here a few properties of these monochromators are outlined through a discussion of their differences.

The four monochromators have different basic structures as follows. The single Wien filter monochromator (a) consists of a Wien filter and an energy-selecting slit; a Wien filter analyses the speed of electrons using the crossing magnetic and electrostatic fields, and the energy-selecting slit mechanically chooses a portion of the dispersed electrons. The double Wien filter monochromator (b) includes two Wien filters with an energy-selecting slit inserted between them. The second Wien filter eliminates the energy dispersion at the conjugate plane of the electron source. The omega-shaped electrostatic monochromator (c) constructs an omega-shaped electron path using four electrostatic toroidal sector deflectors. The latter two deflectors project an achromatic source image. The alpha-type magnetic monochromator (d) is attached after the acceleration tube, and four energy dispersions, which are actually formed by one uniform-field sector (functioning twice) and two gradient-field sectors, are used to produce an alpha-shaped electron path. The omega- or alpha-shaped electron paths minimize the aberrations of each monochromator by acting as in-column energy filters, because the energy-selecting slit and energy dispersion plane of the monochromators lie on the midplane of the electron path.

The electron energy in the energy dispersion part depends on the arrangement of the monochromator and the acceleration tube and yields a critical difference in the monochromator properties. In many cases (i.e. (a)–(c)), the electron energy in the energy dispersion part is relatively low (e.g. a few keV) to obtain sufficient energy dispersion at the energy-selecting slit and, as a result, many monochromators are mounted between the electron gun and the acceleration tube. There are a few technical challenges in mounting a monochromator at a high tension in terms of its electronics, mechanics and the requirement of ultrahigh vacuum in the electron gun chamber. Note that a monochromator at a high tension cannot filter out the instability of the acceleration voltage; however, it can be easily used at various acceleration voltages under the same monochromator condition. The performance of the energy dispersion part depends not only on the electron optics but also on the Boersch effect; therefore, the length of the electron path, the probe current and the number of crossovers should be minimized. In contrast, monochromator (d) attached after the acceleration tube works at the earth ground, and the electron energy in the energy dispersion part is high. Therefore, monochromator (d) requires additional electron optics to magnify the energy dispersion, and NION adopted a multipole lens system as well as a parallel EEL spectrometer or a post-column energy filter [13]. The high-tension instability directly affects the projected position on the energy-selecting slit, allowing us to stabilize the high tension. Monochromator (d) has been combined with a cold field-emission gun (CFEG), which requires ultrahigh vacuum, because monochromator (d) can be fitted on the microscope column below the acceleration tube.

The energy-selecting slit is an indispensable part of a monochromator, and the required slit width is generally of the order of a micrometre. Because monochromators (b) and (c) select electrons at a relatively low energy, the

Table 1. Basic structures of currently available monochromators

	(a) Single Wien filter (FEI)	(b) Double Wien filter (JEOL)	(c) Omega-shaped electrostatic (CEOS)	(d) Alpha-type magnetic (NION)
Basic structure	Wien filter (Acc. tube) Slit	Wien filter Slit Wien filter (Acc. tube)	E-sector x2 Slit E-sector x2 (Acc. tube)	(Acc. tube) M-sector x2 Slit M-sector x2
Electron energy in energy dispersion part	Low	Low	Low	High
Electron energy in energy-selecting slit	High	Low	Low	High
Spatial chromaticity	Residual	Corrected	Corrected	Corrected
Angular chromaticity	Residual	Residual	Corrected	Corrected

Acc. tube, acceleration tube; E-sector, electrostatic toroidal sector deflector; M-sector, magnetic sector.

energy-selecting slit should be clean and free from charge-up. In addition, the mechanical movable components of the energy-selecting slit should not degrade the vacuum in the adjacent electron gun chamber. In contrast, the energy-selecting slits of monochromators (a) and (d) select high-energy electrons in the microscope columns, and a variety of slits and a complicated mechanical/electrical system can be implemented. In the case of the single Wien filter monochromator, the acceleration tube between the Wien filter and the energy-selecting slit magnifies the source image and the energy dispersion, which is advantageous for energy selection. In monochromator (d), a current detection system is implemented on the energy-selecting slit for the additional stabilization of high tension.

Figure 1 shows schematics of the four monochromators, in which the electron path is drawn as a straight line for simplicity. Dotted curves represent the axial paths of electrons with a different energy, and open circles correspond to the source images. Small closed circles are astigmatically focussed (i.e. line-focussed) source images. The multiple energy-dispersive deflectors in monochromators (b)–(d) finally yield an achromatic source image, which is schematically represented as the coincidence of an open circle and a dotted line in Fig. 1b and d. The symmetric optical arrangement of monochromators (c) and (d) yields a symmetric electron path to the midplane at the energy-selecting slit, resulting in the minimized aberration of each system.

Here two types of chromaticity are discussed: spatial chromaticity and angular chromaticity. Spatial chromaticity means that there is energy dispersion at the final source image, which is eliminated in monochromators (b)–(d). Angular chromaticity means that electrons propagating in different directions have different energies, which is eliminated in monochromators (c) and (d) owing to their symmetric electron paths. The effects of these properties on TEM and STEM imaging are discussed later. It is worth mentioning that the angular chromaticity in the double Wien filter monochromator (b) can be controlled by changing the length of the Wien filters. For instance, the deflection induced by the Lorentz force becomes zero (i.e. the

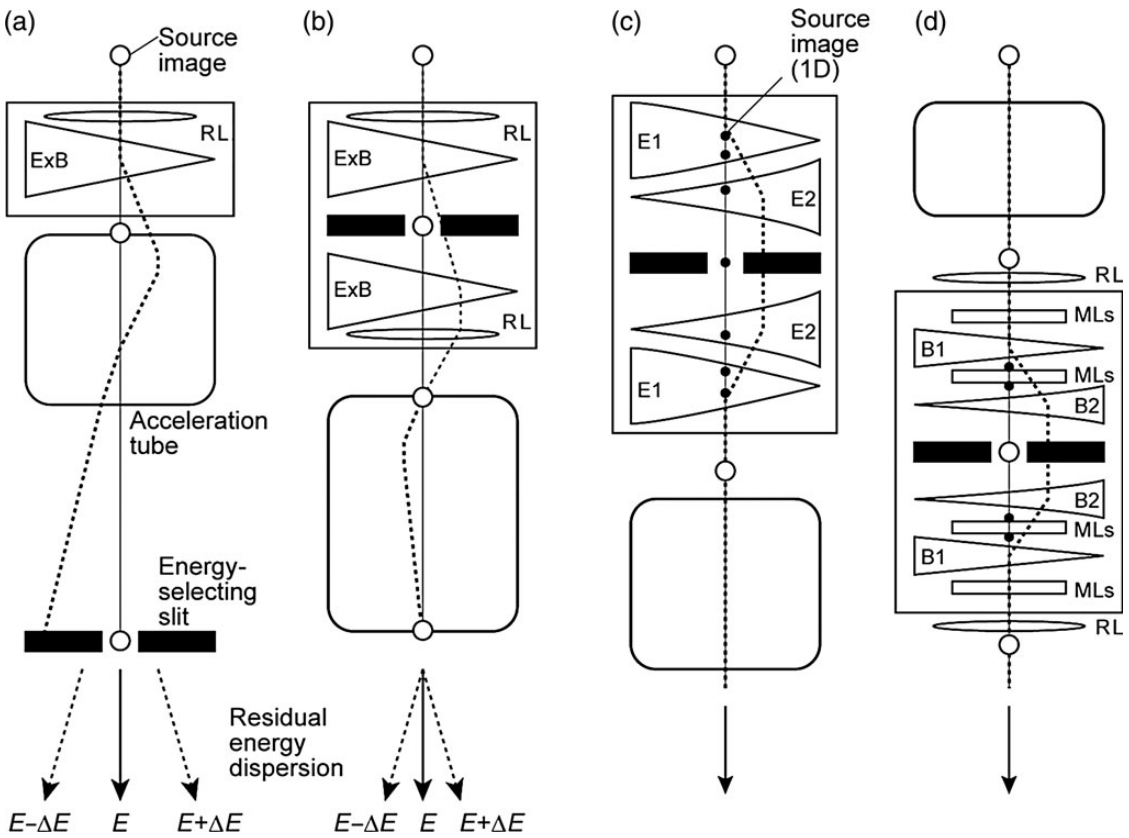

Fig. 1. Schematics of four monochromators: (a) single Wien filter monochromator, (b) double Wien filter monochromator, (c) omega-shaped electrostatic monochromator and (d) alpha-type magnetic monochromator. The electron path with the standard energy is schematically drawn as a straight line, and dotted curves represent the axial paths of electrons with a different energy. Open circles correspond to the conjugate planes to the electron source and small closed circles are the positions of astigmatically focussed (i.e. line-focussed) source images. Rectangles, triangles and rounded rectangles represent monochromator units, energy dispersion parts and acceleration tubes, respectively. The arrows at the bottom represent the residual energy dispersion at the final source image. RL, round lens and MLs, multipole lenses.

rotation angle equals 2π) at a specific filter length, and the angular chromaticity is eliminated under this condition. Figure 1b depicts an example setting, in which the total angle of rotation induced by the Lorentz force equals π, which was reported in a previous paper [8].

Stabilities at a high tension and power supply of the monochromator are critical technical requirements to realize high energy resolution. The high-tension instability cannot be corrected by a monochromator at a high tension, and a highly stabilized high tension is required to realize high energy resolution. Note that a stable energy-dispersed source image on an energy-selecting slit only ensures the stability of the voltage (e.g. a few kV) of the electrons in the monochromator. In contrast, monochromator (d) at the earth ground level can eliminate high-tension instability. Because high-tension instability causes instability in a probe current of monochromator (d), high-tension stability is still required. In addition, a monochromator at the earth ground level requires ultrahigh resolving power in comparison with that of a monochromator at a high tension, and its power supply should also be highly stabilized.

Although the aberration figure on the selecting slit can be easily observed in the single Wien filter monochromator, those of the other monochromators are not observable because of the energy dispersion deflector(s) after the energy-selecting slit, making their alignment indirect. Therefore, an EEL spectrometer is indispensable to align such monochromators. The EEL spectrometer should have high energy resolution (small non-isochromaticity) and be highly stabilized. A few pioneering studies [2] on high-resolution EELS have been performed with the combination of a monochromator and a retarding analyzer, in which the potentials of both energy dispersion deflectors were connected. For this combination, the potential instability does not result in spectroscopic instability, even if the actual energy of incident electrons at the specimen fluctuates. A similar concept is embraced in monochromator (d), in which the power supplies of the monochromator and analyzer are synchronized.

A high-brightness electron gun is preferable for monochromated microscopes. The electron gun brightness is generally defined as the current j per unit solid angle and unit area [A sr^{-1} m^{-2}]. From the viewpoint of monochromated electron microscopy, the brightness of each electron gun should be re-examined on the basis of each energy spread. Namely, the brightness should be normalized by the energy spread (e.g. [A sr^{-1} m^{-2} eV^{-1}]), in which the current j is replaced by the maximum of the energy distribution, $dj(E)/dE$, where E is the energy of the incident electrons. The electron gun brightness related to the energy spread has already been investigated as the *differential brightness* in the theoretical study of Shimoyama and Maruse [14] and as the *reduced brightness* in the experimental study reported by Schwind *et al.* [15]. The latter reported an improvement of the *reduced brightness* in the sharpened tip of a Schottky emission gun (SEG). Because a CFEG has the highest reduced brightness among existing electron guns, the use of a CFEG or SEG with a sharpened tip is preferable for a monochromator.

Monochromators used for EELS

Incident electrons with a narrow energy spread reveal the fine structures of EEL spectra. All the above-mentioned monochromators demonstrate sub-100 meV resolution. An example of the energy distributions obtained using a CFEG and the single Wien filter monochromator is shown in Fig. 2. The energy distribution of a CFEG is limited by the Fermi tail and the tunnelling tail on the low- and high-energy-loss sides, respectively. The Fermi tail has a steep onset comparable to that in our previous report on a monochromator [16,17]; however, recent monochromators have sharp onsets as shown in Fig. 2. This is important because the energy spread of incident electrons should be narrower than the natural Fermi edge of a specimen to reveal the energy-loss near-edge structure of the specimen. Because the tunnelling tail is problematic in the observation of the fine structure in low-energy-loss spectra, monochromators are effective for low-loss spectroscopy. The energy resolution is usually specified by the full width at half maximum (FWHM) of a zero-loss peak; however, the full width at 100th maximum is often appropriate in low-loss spectroscopy. In the practical use of a monochromator, the energy spread, probe current, probe size and convergence angle should be balanced for each purpose. For instance, the

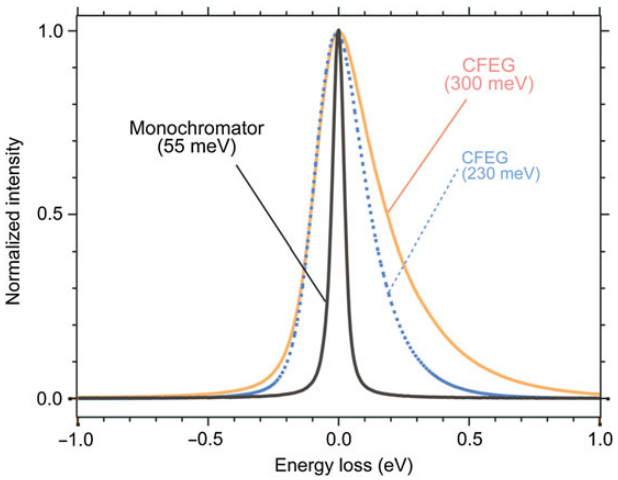

Fig. 2. Energy spreads of the zero-loss peaks of a CFEG and a monochromator. Numbers in parentheses are FWHMs. A narrow energy spread of the monochromator can be realized with a short exposure time of 1 ms. The acceleration voltage of the monochromator is 80 kV.

energy resolution and probe size for atomic-column STEM–EELS elemental mapping should be optimized on the basis of the lifetime energy broadening and the delocalization in inelastic scattering, respectively [18,19]. Otherwise, the low probe current becomes the practical limiting factor preventing the visualization of atomic arrangements in terms of the minimum detectable atomic fraction [1].

In addition to the energy spread of a zero-loss peak, several technical factors should be optimized to realize high energy resolution, such as the stabilities of the high-tension and monochromator power supplies, low-noise circumstances (e.g. stray magnetic field), a narrow point spread function (PSF) of a spectrometer detector and a small chromatic aberration of post-specimen lenses. Conventional techniques for multiple fast acquisition and drift correction [17,20] are still effective even for advanced monochromated microscopy. For instance, the narrow energy spread of the monochromator in Fig. 2 is degraded when a longer exposure time is used. We performed quasi-simultaneous acquisition (e.g. low-loss and core-loss spectra) to accurately evaluate a chemical shift [20], and a similar concept has been commercialized in a more sophisticated product (Gatan, DualEELS). Because the PSF can degrade fine spectral features, a high energy dispersion (e.g. <10 meV ch^{-1}) should be applied, resulting in a narrow energy range (e.g. 200 eV) of an acquired spectrum. A more advanced detector that has a narrow PSF or many channels is preferable. We have recently recognized the last factor, i.e. the effect of the chromatic aberration of the post-specimen lenses, as being particularly important for low-acceleration-voltage electron microscopy. We usually use the drift tube in a spectrometer to switch the energy range, such as from low-loss to high-loss spectroscopy, and we found a substantial difference in each spectroscopic focus, which is due to the vertical shift of the final crossover in the microscope column.

Monochromators used for TEM imaging

The spherical aberration corrector is a breakthrough in TEM [21], yielding the new category of low-voltage high-resolution TEM. Because the third-order spherical aberration coefficient C_3 can be eliminated, the information limit has become more important than the conventional Scherzer limit. There are two envelope functions that restrict the information limit: the spatial envelope K_s and the chromatic envelope K_c [22]. Because C_3 and the optimum defocus become close to zero in C_3-corrected microscopy, the effect of the spatial envelope becomes small even under a convergent illumination condition. Accordingly, the chromatic envelope, which is quantified as the defocus spread, is critical in high-resolution TEM. The defocus spread Δd depends on (i) the energy spread of the incident electrons ΔE, (ii) the high-tension instability ΔV and (iii) the instability of the objective lens current ΔI, and is given as

$$\Delta d = C_c\sqrt{\left(\frac{\Delta E}{E_0}\right)^2 + \left(\frac{\Delta V}{V_0}\right)^2 + \left(\frac{2\Delta I}{I_0}\right)^2}.$$

Monochromators can reduce only the effect of factor (i). However, we demonstrated the advantages of a monochromator in low-voltage high-resolution TEM [23], in which the information limit of 80 kV TEM was improved from about 0.2 nm to 90 pm by reducing the energy spread from 0.9 to 0.1 eV. This means that the energy spread of the incident electrons (i) is a major limiting factor compared with other instabilities (ii) and (iii). Note that the chromatic aberration C_c corrector produces negative chromatic aberration; however, the defocus spread due to the current instability (iii) cannot be eliminated. Thus, the energy-dependent defocus spread (e.g. (i) and (ii)) and the current-dependent defocus spread (iii) should be separately discussed. The current-dependent defocus spread of the C_c corrector system consists of many factors including the current instabilities in the objective lens, the spherical aberration corrector and the C_c corrector itself.

In addition to reducing the energy spread, a monochromator changes the illumination conditions, which affect high-resolution TEM imaging. As mentioned above, some monochromators have a residual energy dispersion, and here the effects of spatial and angular chromaticity on high-resolution TEM are elaborated.

Spatial chromaticity is not critical for high-resolution TEM because each illuminated local area retains a high energy resolution and high-resolution TEM images are acquired with small defocus. The single Wien filter monochromator provides spatial-chromatic illumination, and one of its illumination modes is energy-dispersive critical illumination (so-called rainbow illumination) [6]. Rainbow illumination realizes a high illumination current and local high energy resolution simultaneously. A drawback of rainbow illumination is that the current density on the specimen cannot be changed without degradation of the energy spread. However, this can be easily avoided by using a narrow energy-selecting slit and a defocussed source image, and such a defocussed source with a narrow energy-selecting slit can reduce the convergence angle. An experimental result obtained using such illumination is given later in Fig. 3.

Angular chromaticity exists in monochromators (a) and (b) owing to asymmetric electron paths. Because electrons with different angles have different energies, their TEM images theoretically show different amounts of defocus. If the variation in defocus of each electron is negligible, the

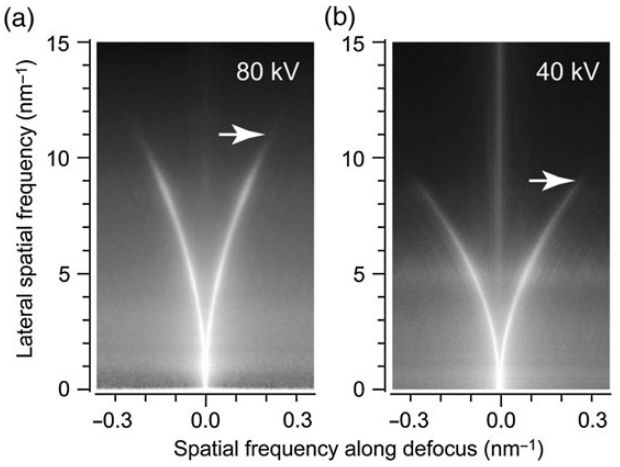

Fig. 3. 3D Fourier transforms of through-focus TEM images at (a) 80 kV and (b) 40 kV. The specimen was an amorphous carbon film. White arcs from the origin correspond to the cross sections of twin Ewald spheres. A monochromated Titan^3 with CETCOR was used. The energy spreads of the TEM imaging were 100 and 60 meV at 80 and 40 kV, respectively. The two arrows show the observable limits of the Ewald spheres, i.e. the information limit.

spatial envelope function under such angular chromaticity is equal to the conventional spatial envelope function. Note that electrons of different directions are considered to be incoherent to each other in the partial coherent imaging theory [24]. In the case of monochromators (a) and (b), the acceleration tube can minimize the angular dispersion; as a result, the angular chromaticity can be minimized. Consequently, spatial/angular chromaticity does not lead to problems in C_3-corrected high-resolution TEM imaging.

The TEM imaging performance can be assessed using the three-dimensional (3D) Fourier transform of through-focus images. Because the experimental through-focus series is considered to be the convolution between a defocus spread function and an ideal (i.e. no defocus spread) through-focus series, the 3D Fourier transform can deduce the defocus spread function as an envelope function. In the 3D Fourier transform data obtained using an amorphous specimen, there are twin Ewald spheres attached at the origin. The information limit can be estimated as the observable lateral frequency in the Ewald spheres. A theoretical outline of this method has been presented elsewhere [25]. Figure 3a and b shows cross sections of 3D Fourier transforms, which were obtained using a monochromated TEM instrument (FEI, Titan^3) with an image corrector (CEOS, CETCOR) and an amorphous carbon film. The white arcs from each origin are the cross sections of twin Ewald spheres. The narrow width of the Ewald spheres indicates parallel illumination. High lateral spatial frequencies of about 11 (90 pm) and 9 nm^{-1} (111 pm) can be observed in the 3D Fourier transforms at 80 and 40 kV, respectively, showing a high information limit. The monochromator is an indispensable instrument for realizing high spatial resolution in low-voltage TEM imaging.

Monochromators used for STEM imaging

Electrons with different energies are defocussed owing to the chromatic aberration of probe-forming lenses, producing a weak and wide tail of the incident probe and resulting in the elongation of the depth of focus and a contrast reduction of annular dark-field (ADF) images. Because the defocus spread does not change the FWHM of the incident probe, the energy spread is not critical to the achievable spatial resolution of STEM ADF imaging.

The demagnified source image projected on the specimen is considered to be spatial incoherent [26], and the geometric size and shape of the projected source limit the achievable spatial resolution. Monochromators (b)–(d), which consist of multiple energy dispersion parts, can construct an achromatic source image; however, the aberration of the monochromator is critical for constructing a circular source image. In the case of the single Wien filter monochromator, various slits or apertures can be inserted on the energy-dispersed source image, because the energy-selecting slit units are located in the microscope column at the earth ground. The aperture is thus a source for the following STEM optics. Using a circular aperture (e.g. an aperture of 1 μm diameter), the source image projected on the specimen always becomes circular even when the monochromator is misaligned. An example of monochromated STEM imaging is shown in Fig. 4, where the images were obtained using the single Wien filter monochromator at an acceleration voltage of 300 kV (FEI, Titan^3). A $SrTiO_3$ (001) specimen was prepared by mechanical thinning and Ar ion milling (Gatan, PIPS and Technoorg-Linda, GentleMill). An ADF image with a high signal-to-noise ratio was observed using a multiple fast acquisition and drift correction technique [27,28]. The Fourier transform of the ADF image (Fig. 4a) shows no anisotropy, and a spatial frequency of about 70 pm is observed. The illumination conditions, such as the probe current, probe size and energy spread, can be changed via a variety of instrument parameters including the spot size (i.e. demagnification in the condenser lens system), convergence angle, energy dispersion and energy slit width of the monochromator. The settings of the instrument used to obtain Fig. 4a and d realize a high probe current (56 pA) and high spatial resolution (70 pm) with a moderate energy resolution (0.15 eV), which are suitable conditions for element-selective atomic-column imaging using STEM–EELS.

Under a high-demagnification condition of the condenser lens system, small-angle electrons emitted from the electron source are selected by the objective aperture. As a result, the angular chromaticity becomes negligible. In other words,

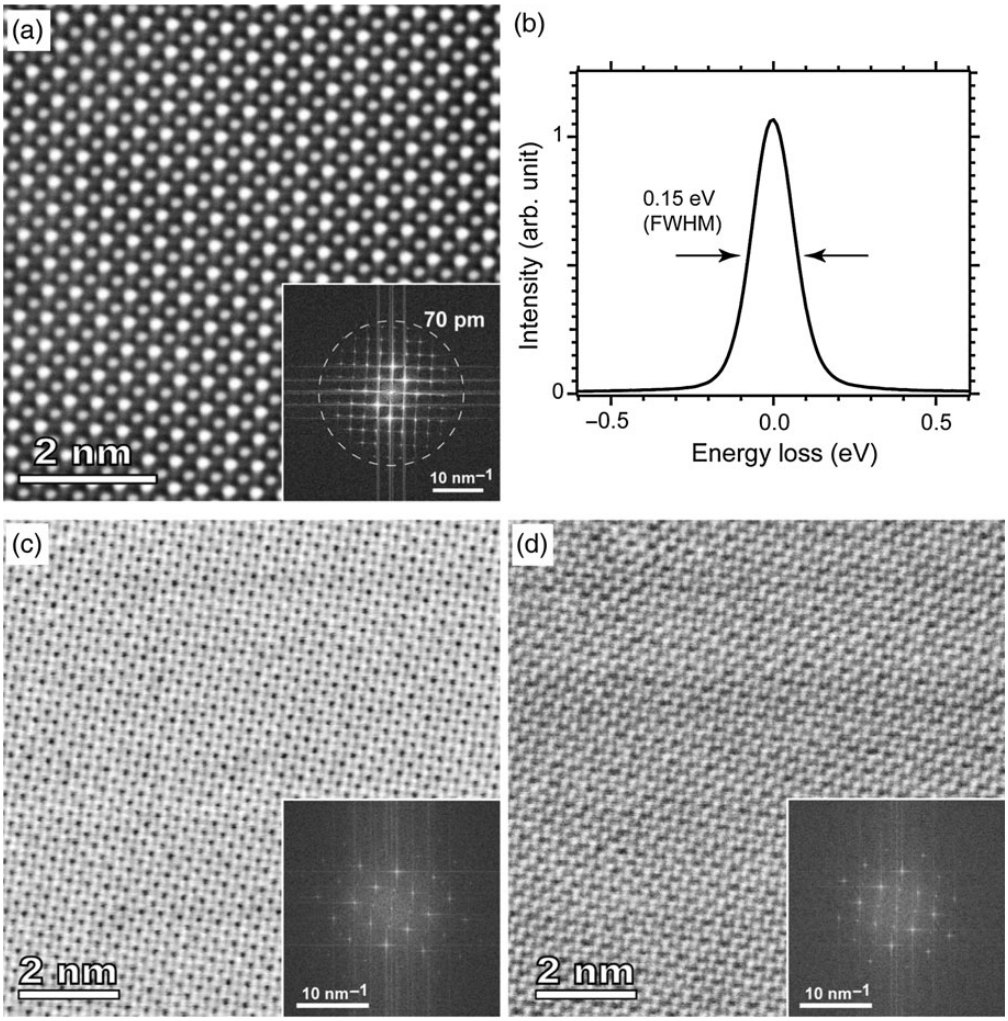

Fig. 4. Example of monochromated STEM imaging. The specimen is (001) $SrTiO_3$. Titan[3] with a probe corrector and a monochromator was used at 300 kV. (a) ADF image, (b) zero-loss peak, (c) ABF image and (d) BF image. A high probe current (56 pA) and high spatial resolution (70 pm) with a moderate energy resolution (0.15 eV) are simultaneously realized.

the objective aperture of the probe-forming lens is coherently illuminated even in the case of angular chromaticity. Note that a coherently illuminated objective aperture is necessary for reciprocity, which is fundamental for the interpretation of bright-field (BF) STEM image contrast. Under such high-resolution STEM imaging conditions, BF STEM images can be acquired as well as conventional STEM images. Figure 4c and d shows annular bright-field (ABF) and BF images, respectively, where a low-pass filter is applied. Both images also show isotropic imaging properties. Thus, STEM imaging is not degraded by using the currently available monochromators.

Concluding remarks

The practical aspects of monochromators developed for electron microscopes have been reviewed. Four monochromators, the single Wien filter monochromator, the double Wien filter monochromator, the omega-shaped electrostatic monochromator and the alpha-shaped magnetic monochromator, were compared. A few critical properties of the monochromators, such as spatial and angular chromaticity, were discussed. The advantages and side effects of the monochromators in EEL spectroscopy and TEM and STEM imaging were pointed out. The monochromators are effective not only for EEL spectroscopy but also for high-resolution TEM imaging, and spatial/angular chromaticity is not problematic in TEM and STEM imaging.

The monochromator is one of the frontiers of advanced electron microscopy, and other techniques such as the use of a spin-polarized electron gun and a pulsed electron gun are promising techniques. A monochromator for surface analysis has already achieved 1 meV resolution in a unified system consisting of a monochromator and a spectrometer, and there is still room for an improvement of monochromators for electron microscopy.

Acknowledgements

The author thanks Dr Tiemeijer, Dr Lazar, Mr Matsumoto, Dr Bright, Dr Inoke, Dr van Cappellen and Dr Freitag for advice on the monochromator, and Dr Krivanek, Dr Mukai, Dr Saito, Dr Suenaga, Prof. Hirayama and Prof. Ikuhara for useful discussions on their monochromators. The author also thanks Dr Nagai, Mr Kurashima, Ms Ohwada, Dr Koshiya and Dr Kikkawa for carrying out monochromator experiments and Dr Ishizuka for invaluable discussions on imaging theory.

Funding

This study was partly supported by the JST Research Acceleration Program and the Nano Platform Program of MEXT, Japan. Funding to pay the Open Access publication charges for this article was provided by National Institute for Materials Science.

References

1. Egerton R F (2011) *Electron Energy-Loss Spectroscopy in the Electron Microscope*, 3rd edn. (Plenum Press, New York).
2. Terauchi M, Kuzuo R, Satoh F, Tanaka M, Tsuno K, Ohyama J (1991) Performance of a new high-resolution electron energy-loss spectroscopy microscope. *Microsc. Microanal. Microstruct.* 2: 351–358.
3. Tsuno K (2011) Monochromators in electron microscopy. *Nucl. Instrum. Methods A* 645: 12–19.
4. Mook H W, Kruit P (2000) Construction and characterization of the fringe field monochromator for a field emission gun. *Ultramicroscopy* 81: 129–139.
5. Tiemeijer P C, Bischoff M, Freitag B, Kisielowski C (2012) Using a monochromator to improve the resolution in TEM to below 0.5 Å. Part II: application to focal series reconstruction. *Ultramicroscopy* 118: 35–43.
6. Tiemeijer P C, Bischoff M, Freitag B, Kisielowski C (2012) Using a monochromator to improve the resolution in TEM to below 0.5 Å. Part I: creating highly coherent monochromated illumination. *Ultramicroscopy* 114: 72–81.
7. Tiemeijer P C (1999) Operation modes of a TEM monochromator. *Inst. Phys. Conf. Ser.* 161: 191–194.
8. Mukai M, Kim J S, Omoto K, Sawada H, Kimura A, Ikeda A, Zhou J, Kaneyama T, Young N P, Warner J H, Nellist P D, Kirkland A I (2014) The development of a 200 kV monochromated field emission electron source. *Ultramicroscopy* 140: 37–43.
9. Rose H (1999) Prospects for realizing a sub-angstrom sub-eV resolution EFTEM. *Ultramicroscopy* 78: 13–25.
10. Essers E, Benner G, Mandler T, Meyer S, Mittmann D, Schnell M, Hoschen R (2010) Energy resolution of an omega-type monochromator and imaging properties of the MANDOLINE filter. *Ultramicroscopy* 110: 971–980.
11. Krivanek O L, Lovejoy T C, Dellby N, Carpenter R W (2013) Monochromated STEM with a 30 meV-wide, atom-sized electron probe. *Microscopy* 62: 3–21.
12. Krivanek O L, Ursin J P, Bacon N J, Corbin G J, Dellby N, Hrncirik P, Murfitt M F, Own C S, Szilagyi Z S (2009) High-energy-resolution monochromator for aberration-corrected scanning transmission electron microscopy/electron energy-loss spectroscopy. *Philos. Trans. R. Soc. London. Sec. A* 367: 3683–3697.
13. Krivanek O L, Gubbens A J, Dellby N (1991) Developments in EELS instrumentation for spectroscopy and imaging. *Microsc. Microanal. Microstruct.* 2: 315–332.
14. Shimoyama H, Maruse S (1984) Theoretical considerations on electron-optical brightness for thermionic, field and T-F emissions. *Ultramicroscopy* 15: 239–254.
15. Schwind G A, Magera G, Swanson L W (2006) Comparison of parameters for Schottky and cold field emission sources. *J. Vac. Sci. Technol. B* 24: 2897–2901.
16. Kimoto K, Kothleitner G, Grogger W, Matsui Y, Hofer F (2005) Advantages of a monochromator for bandgap measurements using electron energy-loss spectroscopy. *Micron* 36: 185–189.
17. Kimoto K, Ishizuka K, Asaka T, Nagai T, Matsui Y (2005) 0.23 eV energy resolution obtained using a cold field-emission gun and a streak imaging technique. *Micron* 36: 465–469.
18. Kimoto K, Asaka T, Nagai T, Saito M, Matsui Y, Ishizuka K (2007) Element-selective imaging of atomic columns in a crystal using STEM and EELS. *Nature* 450: 702–704.
19. Kimoto K, Ishizuka K, Matsui Y (2008) Decisive factors for realizing atomic-column resolution using STEM and EELS. *Micron* 39: 257–262.
20. Kimoto K, Matsui Y (2002) Software techniques for EELS to realize about 0.3 eV energy resolution using 300 kV FEG-TEM. *J. Microsc.* 208: 224–228.
21. Haider M, Uhlemann S, Schwan E, Rose H, Kabius B, Urban K (1998) Electron microscopy image enhanced. *Nature* 392: 768–769.
22. Reimer L, Kohl H (2008) *Transmission Electron Microscopy*, 5th edn. (Springer, New York).
23. Kimoto K, Kurashima K, Nagai T, Ohwada M, Ishizuka K (2012) Assessment of lower-voltage TEM performance using 3D Fourier transform of through-focus series. *Ultramicroscopy* 121: 31–37.
24. Ishizuka K (1980) Contrast transfer of crystal images in TEM. *Ultramicroscopy* 5: 55–65.
25. Kimoto K, Sawada H, Sasaki T, Sato Y, Nagai T, Ohwada M, Suenaga K, Ishizuka K (2013) Quantitative evaluation of temporal partial coherence using 3D Fourier transforms of through-focus TEM images. *Ultramicroscopy* 134: 86–93.
26. LeBeau J M, Findlay S D, Allen L J, Stemmer S (2008) Quantitative atomic resolution scanning transmission electron microscopy. *Phys. Rev. Lett.* 100: 206101.
27. Kimoto K, Asaka T, Yu X, Nagai T, Matsui Y, Ishizuka K (2010) Local crystal structure analysis with several picometer precision using scanning transmission electron microscopy. *Ultramicroscopy* 110: 778–782.
28. Saito M, Kimoto K, Nagai T, Fukushima S, Akahoshi D, Kuwahara H, Matsui Y, Ishizuka K (2009) Local crystal structure analysis with 10-pm accuracy using scanning transmission electron microscopy. *J. Electron Microsc.* 58: 131–136.